

## Neutron Diffraction and EM Structure Determination of the Oxide $\text{PbBa}_{0.8}\text{Sr}_{1.2}\text{PrCeCu}_3\text{O}_9$ , a Perfectly Ordered Intergrowth of Rock Salt, Oxygen-Deficient Perovskite, and Fluorite-Type Structures

T. ROUILLON, V. CAIGNAERT, C. MICHEL, M. HERVIEU,  
D. GROULT, AND B. RAVEAU

*Laboratoire CRISMAT, Bd du Maréchal Juin, 14050 Caen Cédex, France*

Received April 7, 1991

The structure of  $\text{PbBa}_{0.8}\text{Sr}_{1.2}\text{PrCeCu}_3\text{O}_9$  has been determined with powder neutron diffraction techniques and profile analysis. The symmetry of this oxide is pseudotetragonal  $P4mm$ , but ED study shows that it is orthorhombic, space group  $Cmm2$ , with cell parameters  $a = 5.4816(1) \text{ \AA}$ ,  $b = 5.4703(1) \text{ \AA}$ , and  $c = 16.4017(4) \text{ \AA}$ . The structure of this oxide corresponds to a triple intergrowth of single and double oxygen-deficient perovskite layers, with single rock salt and double fluorite-type layers. The analysis of the structure does not show any statistical distribution of copper and lead in the same sites, contrary to what was found for similar compositions. The main original structural features are: (a) the disordered distribution of oxygen in the  $\text{PbO}$  layers and the distorted tetrahedral coordination of lead  $\text{PbO}_3\text{L}$  due to the  $6s^2$  lone pair of  $\text{Pb(II)(L)}$ ; (b) the angle of the  $\text{O-Cu-O}$  bond of univalent copper ( $164^\circ$ ); (c) the off-centering of rare earth elements in the " $\text{O}_8$ " cages, which move away from the copper layers; and (d) the displacement of  $\text{Cu(II)}$  inside the  $\text{CuO}_5$  pyramids toward the apical oxygen. A comparison with  $\text{Pb}_2\text{Sr}_2\text{YCu}_3\text{O}_8$ -type structures is made. © 1992 Academic Press, Inc.

### Introduction

The analysis of superconducting copper oxides involving double pyramidal copper layers shows that calcium or yttrium ions and the oxygens of the basal planes form a layer of edge-sharing distorted  $\text{AO}_8$  ( $A = \text{Ca, Y}$ ) cubes similar to those observed in the fluorite structure (Fig. 1a). The possibility of replacing these single fluorite-type layers by double layers was first demonstrated with the synthesis of the oxides  $\text{Tl}_{1-x}\text{A}_{2-y}\text{Ln}_2\text{Cu}_2\text{O}_9$  (1) with  $\text{Ln} = \text{Pr, Nd, Ce}$ , and  $A = \text{Sr, Ba}$ , and  $\text{Nd}_{2.64}\text{Sr}_{0.82}\text{Ce}_{0.54}\text{Cu}_2\text{O}_8$  (2, 3). These two structures correspond to the replacement of single  $[\text{CaO}_2]_\infty$  layers by double  $[\text{Ln}_2\text{O}_4]_\infty$  layers (Fig. 1b) in the  $\text{TlBa}_2\text{CaCu}_2\text{O}_7$  structure and in the  $\text{La}_2\text{CaCu}_2\text{O}_6$

structure, respectively. A generalization of this concept to all the copper oxides involving double pyramidal copper layers allowed new triple intergrowths of rock salt, oxygen-deficient perovskite, and fluorite-type structures to be isolated (4–7). Within this series, we undertook recently the synthesis of the oxide  $\text{PbBa}_{1-x}\text{Sr}_{1+x}\text{PrCeCu}_3\text{O}_9$ , which was susceptible to correspond to the replacement of a  $[\text{YO}_2]_\infty$  layer by a  $[\text{Ln}_2\text{O}_4]_\infty$  layer in the  $\text{BaPbYSrCu}_3\text{O}_7$  structure (Fig. 2). At the end of our work, Tokiwa *et al.* (8) published a paper on very similar compounds  $\text{PbBa}_{0.7}\text{Sr}_{1.3}\text{LnCeCu}_3\text{O}_9$  with  $\text{Ln} = \text{Sm, Eu, Gd}$ , which we found to be isostructural with our oxide. However, the structural model proposed by these authors appeared to us as questionable, since they proposed the

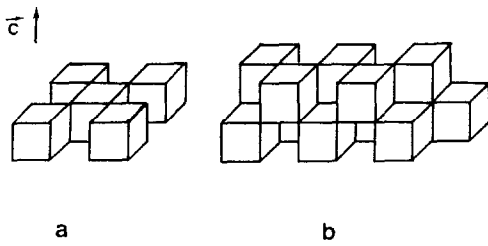


FIG. 1. Idealized drawing of (a) a single layer of edge sharing  $AO_8$  cubes ( $A = \text{Ca}, \text{Y}$ ) intercalated between the pyramidal copper layers in the superconducting copper oxides; (b) double fluorite layer  $[\text{Ln}_2\text{O}_4]_x$ .

presence of copper and divalent lead on the same crystallographic sites. Unfortunately the space group and the atomic positions given by the authors were revealed to be incompatible with their structural model so that it is not possible to obtain a clean description of the structure. We report here on the structure of the oxide  $\text{PbBa}_{0.8}\text{Sr}_{1.2}\text{PrCeCu}_3\text{O}_9$ , which we determined by powder neutron diffraction and studied by electron microscopy.

### Experimental

Samples were prepared by mixing and grinding  $\text{PbO}$ ,  $\text{SrCuO}_2$ ,  $\text{BaCuO}_2$ ,  $\text{Cu}_2\text{O}$ ,

$\text{Pr}_6\text{O}_{11}$ , and  $\text{CeO}_2$  in stoichiometric ratios according to the formulation  $\text{PbBa}_{1-x}\text{Sr}_{1+x}\text{PrCeCu}_3\text{O}_9$ . The mixtures were sintered at  $830^\circ\text{C}$  in nitrogen flow for 64 hr and quenched to room temperature. The samples were characterized by X-ray powder diffraction and electron diffraction in order to test their homogeneity. Electron diffraction was performed with a JEOL 120 KV microscope equipped with a side-entry goniometer ( $\pm 60^\circ$ ). The neutron diffraction pattern was registered at room temperature on the high-resolution diffractometer D2b at ILL, using a wavelength of  $1.594 \text{ \AA}$ . Intensities were measured between  $5^\circ$  and  $160^\circ$  ( $2\theta$ ) with increments of  $0.05^\circ$ . The structure was refined between  $15^\circ$  and  $155^\circ$  ( $2\theta$ ) with the Rietveld method using a modified version of the DBW3.2S program (14). For calculation peak shape was assumed to be Gaussian. X-ray powder diffraction data were registered on a Philips diffractometer for  $\text{CuK}\alpha$  radiation.

High resolution electron microscopy was carried out with a JEOL 200 CX microscope equipped with a top-entry ( $\pm 10^\circ$ ) double tilt goniometer and an objective lens with a spherical aberration constant of  $0.8 \text{ mm}$ . The specimen were prepared by grinding,

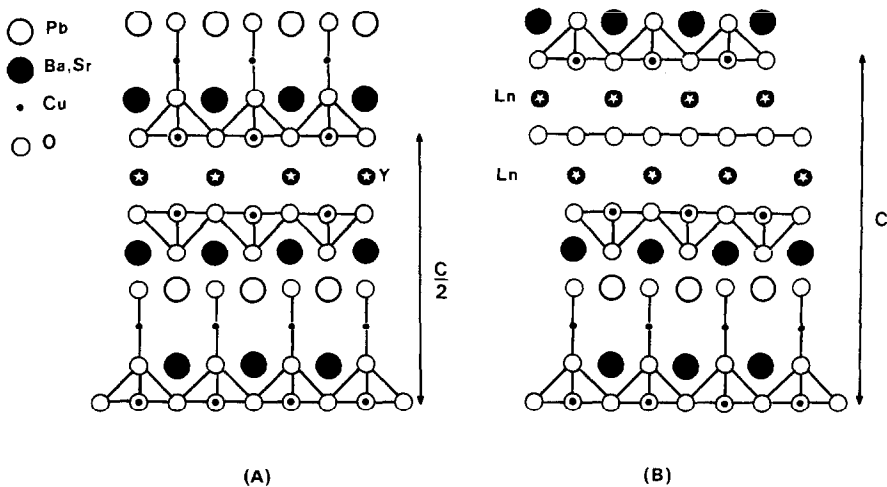


FIG. 2. Idealized projection of the structure of (A)  $\text{PbBaSrYCu}_3\text{O}_7$ ; (B)  $\text{PbBa}_{1-x}\text{Sr}_{1+x}\text{PrCeCu}_3\text{O}_9$ .

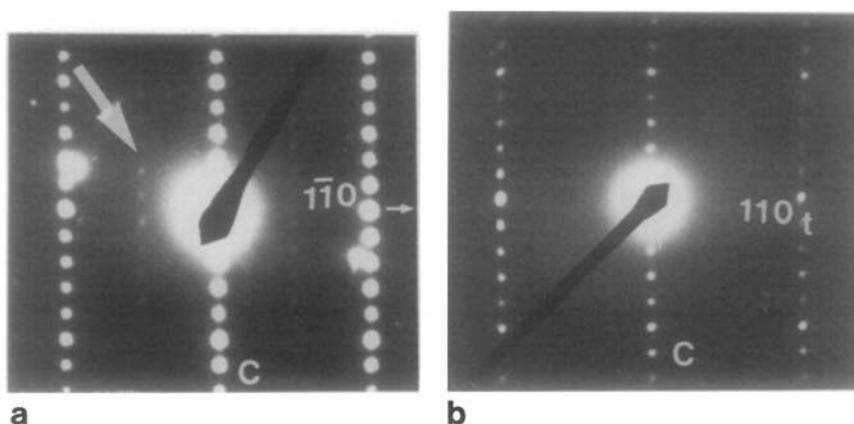


FIG. 3.  $[110]_T$  and  $[\bar{1}\bar{1}0]_T$  electron diffraction patterns. The first one exhibits weak reflections (large white arrows), contrary to the second one.

and the small crystals suspended in butanol were deposited on carbon coated holey films supported by a Cu grid.

## Results

According to the above mentioned experimental conditions, a pure phase was isolated for the composition  $\text{PbBa}_{0.8}\text{Sr}_{1.2}\text{PrCeCu}_3\text{O}_9$ . The parameters of the tetragonal cell and reflection conditions were determined from electron diffraction and X ray diffraction data to be  $a = 3.8717(1) \text{ \AA}$  and  $c = 16.3986(6) \text{ \AA}$ . No reflection conditions were observed, leading to the following possible space groups:  $P4$ ,  $P4$ ,  $P4/m$ ,  $P422$ ,  $P4mm$ ,  $P42m$ ,  $P4m2$ , and  $P4/mmm$ .

### Electron Diffraction Study

More than 50 crystals were studied by electron diffraction, reconstructing the reciprocal space. This systematic investigation showed that all the crystals exhibit strong reflections corresponding to a tetragonal unit cell with  $a = 3.87 \text{ \AA}$ ,  $c = 16.40 \text{ \AA}$ , and no reflection conditions.

However long exposures revealed the existence of very weak reflections as shown in Fig. 3. These weak reflections are observed

in the  $[110]_T$  zone axis patterns ( $_T$  refers to the tetragonal cell), whereas they are not observed in the  $[\bar{1}\bar{1}0]_T$  patterns, involving an orthorhombic symmetry. The appearance of these extra spots is not systematic, suggesting that the responsible phenomenon varies from one crystal to the other. The  $[110]_T$  pattern exhibit spots in position  $(\frac{1}{2}, \frac{1}{2}, \frac{1}{2})$  with respect to the tetragonal cell (Fig. 3a), however, broad streaks are often observed along the  $c^*$  axis (Fig. 3b), showing that the ordering is not perfect over long distances and that no real periodicity is observed in that direction; in that way, a supercell  $a' \approx a_T\sqrt{2}$ ,  $b' \approx a_T\sqrt{2}$ , and  $c' \approx c$  can be used to describe these patterns.

### Determination of the Structure by Neutron Diffraction

The starting structural parameters used for the analysis of the neutron diffraction data were deduced from our structural model (Fig. 2b), in which single and double copper layers are intergrown with single rock-salt-type layers and double fluorite-type layers. The preliminary X-ray diffraction structure calculations allowed the positions of the metallic atoms to be confirmed. The neutron diffraction studies were then

TABLE I  
REFINED STRUCTURAL PARAMETERS FOR  $\text{PbBa}_{0.77}\text{Sr}_{1.23}\text{PrCeCu}_3\text{O}_9$ : SPACE GROUP  $P4mm$  (NO. 99),  
 $Z = 1$ ,  $a = b = 3.8721(1)$  Å,  $c = 16.4017(4)$  Å

Atom	Position	$x/a$	$y/b$	$z/c$	$B(\text{Å}^2)$	$\tau$ (occ. fact)
Pb	1a	0	0	0	1.40(17)	0.93(2)
Sr, Ba <sub>1</sub>	1b	$\frac{1}{2}$	$\frac{1}{2}$	0.1582(17)	1.36(18)	0.76/0.24 <sup>c</sup>
Cu <sub>1</sub>	1a	0	0	0.2722(7)	0.54(9)	1 <sup>d</sup>
$Ln_1$ : Pr,Ce	1b	$\frac{1}{2}$	$\frac{1}{2}$	0.3832(7)	0.06(8) <sup>b</sup>	0.5/0.5 <sup>d</sup>
$Ln_2$ : Pr,Ce	1a	0	0	0.5402(6)	0.06(8) <sup>b</sup>	0.5/0.5 <sup>d</sup>
Cu <sub>2</sub>	1b	$\frac{1}{2}$	$\frac{1}{2}$	0.6500(5)	0.44(12)	1 <sup>d</sup>
Sr, Ba <sub>2</sub>	1a	0	0	0.7567(6)	0.52(17)	0.47/0.53 <sup>c</sup>
Cu <sub>3</sub>	1b	$\frac{1}{2}$	$\frac{1}{2}$	0.8996(5)	1.86(20)	1 <sup>d</sup>
O <sub>1</sub> <sup>a</sup>	4f	0.6359(23)	$\frac{1}{2}$	0.0056(7)	0.97(24)	0.25 <sup>d</sup>
O <sub>2</sub>	1a	0	0	0.1281(10)	2.44(26) <sup>e</sup>	1 <sup>d</sup>
O <sub>3</sub>	2c	$\frac{1}{2}$	0	0.2770(5)	1.18(13)	1 <sup>d</sup>
O <sub>4</sub>	2c	$\frac{1}{2}$	0	0.4565(7)	1.41(6)	1 <sup>d</sup>
O <sub>5</sub>	2c	$\frac{1}{2}$	0	0.6288(4)	0.73(11)	1 <sup>d</sup>
O <sub>6</sub>	1b	$\frac{1}{2}$	$\frac{1}{2}$	0.7841(9)	1.78(21)	1 <sup>d</sup>
O <sub>7</sub>	2c	$\frac{1}{2}$	0	0.8996 <sup>f</sup>	1.00 <sup>f</sup>	0 <sup>d</sup>
O <sub>8</sub>	1a	0	0	0.8996 <sup>f</sup>	1.00 <sup>f</sup>	0 <sup>d</sup>

Note.  $R_p = 5.55\%$ ,  $R_{wp} = 7.19\%$ ,  $R_{exp} = 2.75\%$ ,  $R_i = 5.91\%$ ,  $R_f = 4.96\%$ .

<sup>a</sup> Deviated from the (1b) position [ $\frac{1}{2}$ ,  $\frac{1}{2}$ , 0.0056].

<sup>b</sup> Refined simultaneously.

<sup>c</sup> Fixed from the X-ray powder diffraction refinement.

<sup>d</sup> Refined in first step and fixed after.

<sup>e</sup> Refined also in the (4e) position: [0.0677(35), 0, 0.1261(7)],  $B = 0.22(29)$  Å<sup>2</sup>, and  $\tau = 0.25$ , but does not give significant improvement for the reliability factors.

<sup>f</sup> Empty positions at Cu<sub>3</sub> level.

performed in a first step on 191  $hkl$  reflections allowed by the  $P4mm$  space group. The cationic and anionic positions and isotropic thermal factors were refined successively. After refinement, six oxygen sites (O<sub>1</sub> to O<sub>6</sub>) were found to be fully occupied, whereas the O<sub>7</sub> and O<sub>8</sub> sites, located at the same level as Cu<sub>3</sub>, were found to be empty. All the isotropic thermal factors were found to be acceptable, except that of O<sub>1</sub>, which was found to be extremely high ( $B \approx 11$  Å<sup>2</sup>). Thus a splitting of the 1(b) site of O<sub>1</sub> into a 4(f) site with an occupancy factor of 0.25 was considered. The latter position was easily refined leading to a significant improvement of the  $R_i$  factor. The refined parameters given in Table I correspond to satisfactory reliability factors  $R_{wp} = 7.19\%$ ,  $R_{exp} = 2.75\%$ , and  $R_i = 5.91\%$ . Neverthe-

less, the comparison of the calculated and observed patterns shows their difference is not absolutely perfect for  $2\theta$  angles superior to 110° (Fig. 4a). Taking into account the electron diffraction results, calculations were performed finally in the orthorhombic space group  $Cmm2$  ( $a \approx b \approx a_T\sqrt{2}$ ) (299  $hkl$  reflections) according to the structural model given in Fig. 5. The refinement of the cell parameters leads to a significant orthorhombic distortion:  $a = 5.4816(1)$  Å,  $b = 5.4703(1)$  Å, and  $c = 16.0417(4)$  Å. The refined positions (Table II) are close to those observed in the tetragonal group, so that they do not affect significantly the interatomic distances and angles (Table III). One can notice that the calculated neutron diffraction pattern is now in better agreement with the experimental pattern (Fig. 4b).

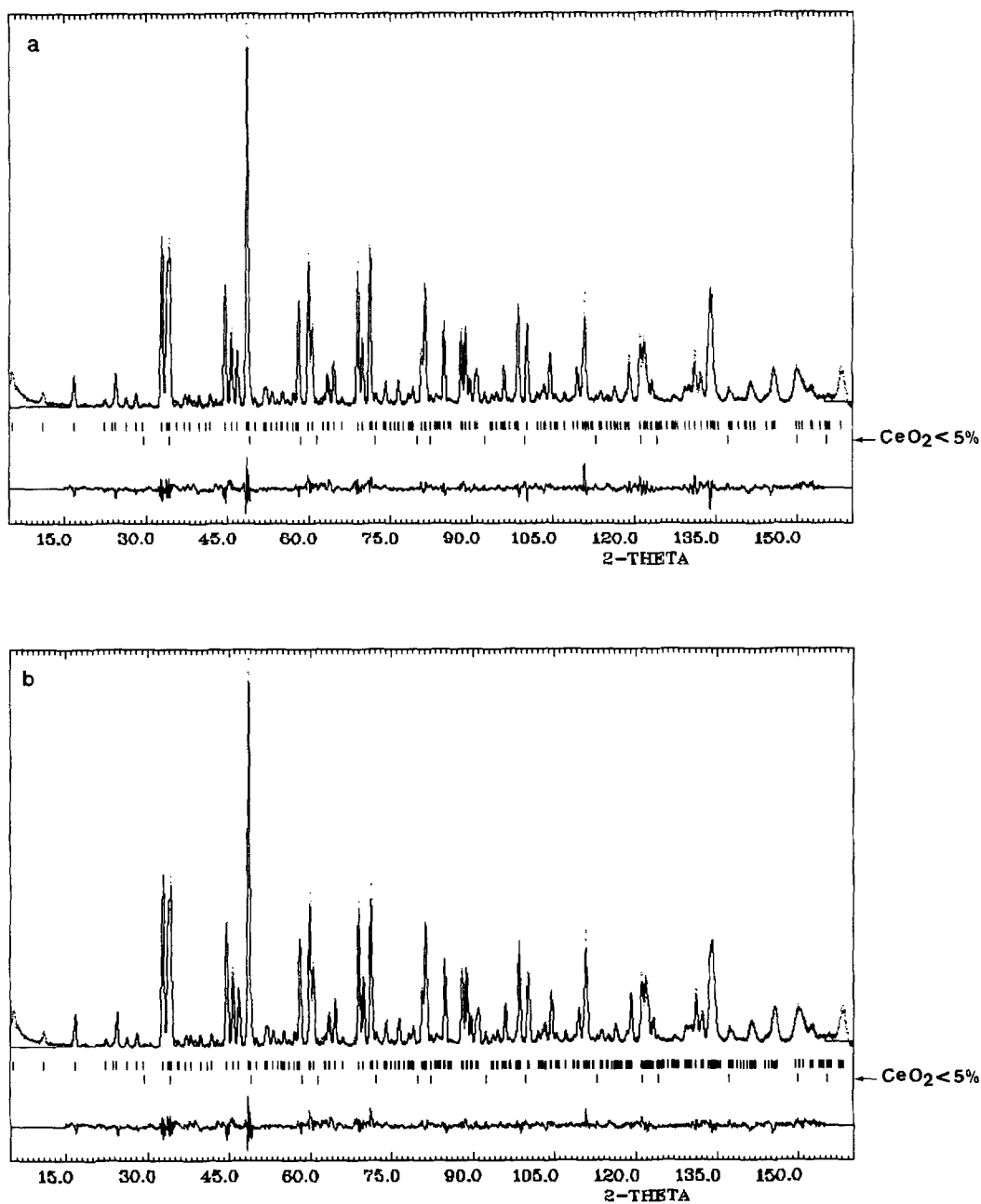


FIG. 4. Experimental and calculated neutrons diffraction profiles and their difference for (a) tetragonal symmetry, space group  $P4mm$ ; (b) orthorhombic symmetry, space group  $Cmm2$ .

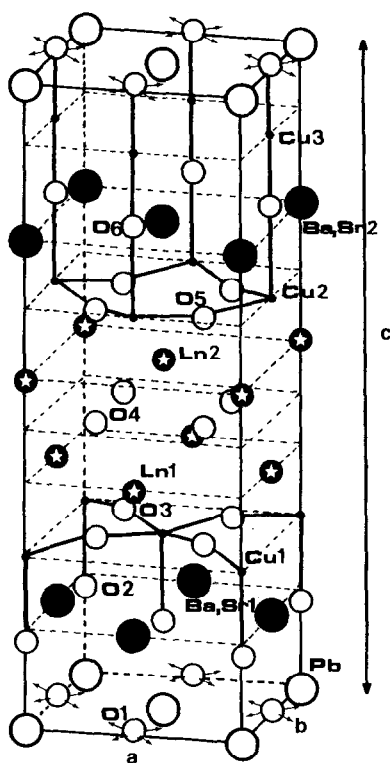


FIG. 5. Structural model for the orthorhombic oxide  $\text{PbBa}_{0.8}\text{Sr}_{1.2}\text{PrCeCu}_3\text{O}_9$  (refined composition  $\text{PbBa}_{0.77}\text{Sr}_{1.23}\text{PrCeCu}_3\text{O}_9$ ).

Attempts to refine the anisotropic thermal factors did not allow better results to be obtained for  $P4mm$  or  $Cmm2$  space groups.

### Description of the Structure and Discussion

These results show that the structure of  $\text{PbBa}_{0.8}\text{Sr}_{1.2}\text{PrCeCu}_3\text{O}_9$  consists of a regular intergrowth of single and double oxygen-deficient perovskite layers formulated  $[\text{ACuO}_{2.5}\square_{0.5}]_\infty$  and  $[\text{ACu}_2\text{O}_3\square_3]_\infty$ , respectively, with double fluorite-type layers  $[\text{Ln}_2\text{O}_4]_\infty$  and single rock-salt-type layers  $[\text{A}_{0.5}\text{Pb}_{0.5}\text{O}]_\infty$  ( $A = \text{Sr}, \text{Ba}$ ).

Contrary to what was previously claimed for  $\text{PbBa}_{0.7}\text{Sr}_{1.3}\text{LnCeCu}_3\text{O}_9$  (8), we do not

observe any statistical distribution of copper and lead on the same crystallographic sites. The  $\text{Cu}_3$  sites are indeed fully occupied by copper, whereas the occupancy factor of Pb sites suggests a small lead deficiency which can be explained by  $\text{PbO}$  loss during synthesis.

This very regular character of the structure is confirmed by HREM (Fig. 6), which shows a very regular contrast in all the crystals, ruling out the existence of shifted microdomains, contrary to what was proposed for  $\text{PbBa}_{0.7}\text{Sr}_{1.3}\text{LnCeCu}_3\text{O}_9$  (8).

The second important point deals with the oxygen content and distribution. The " $\text{O}_9$ " composition is indeed confirmed, with a total absence of oxygen at the level of  $\text{Cu}_3$ . Moreover the splitting of the  $\text{O}_1$  oxygens shows that there exists a disordered distribution of oxygen in the  $[\text{PbO}]_\infty$  layers, similar to that observed in  $\text{Pb}_2\text{Sr}_2\text{YCu}_3\text{O}_8$ -type oxides (9–11). This oxygen distribution suggests that this oxide is characterized by the mixed valency  $\text{Cu(II)/Cu(I)}$ , according to the ideal formula  $\text{Pb}^{\text{II}}\text{Ba}_{0.8}\text{Sr}_{1.2}\text{Pr}^{\text{III}}\text{Ce}^{\text{IV}}\text{Cu}_2^{\text{II}}\text{Cu}_1^{\text{I}}\text{O}_9$ . Bond valence calculations (12, 13) are in agreement with the latter formula, since one obtains mean charges of +1.9 for Pb, +2.0 and +2.1 for  $\text{Cu}_2$  and  $\text{Cu}_1$ , respectively, 1.0 for  $\text{Cu}_3$ , and +3.5 for both lanthanide sites.

The examination of the interatomic distances (Table III) allows the following comments to be made:

(i) The " $\text{O}_4$ " basal planes of the  $\text{Cu}_1$  and  $\text{Cu}_2$  pyramids are almost perfectly square.  $\text{Cu}_1$  as well as  $\text{Cu}_2$  form four equal Cu–O distances with the four oxygens of 1.94 and 1.97 Å, respectively, i.e., close to those generally observed for superconducting cuprates. The main difference with high  $T_c$  cuprates deals with the fact that copper is significantly displaced out of the " $\text{O}_4$ " plane toward the center of the  $\text{CuO}_3$  pyramid (Figs. 7a,b) of 0.1 to 0.35 Å. This leads to much shorter apical Cu–O distances (2.21–

TABLE II  
REFINED STRUCTURAL PARAMETERS FOR  $\text{PbBa}_{0.77}\text{Sr}_{1.23}\text{PrCeCu}_3\text{O}_9$ : SPACE GROUP  $Cmm2$  (NO. 35),  
 $Z = 2$ ,  $a = 5.4816(1)$ ,  $b = 5.4703(1)$ , and  $c = 16.4017(4)$  Å

Atom	Position	$x/a$	$y/b$	$z/c$	$B$ (Å <sup>2</sup> )	$\tau$ (occ. fact)
Pb	$2a$	0	0	0	1.51(16)	0.95(2)
Sr, Ba <sub>1</sub>	$2b$	$\frac{1}{2}$	0	0.1581(6)	1.43(16)	0.76/0.24 <sup>c</sup>
Cu <sub>1</sub>	$2a$	0	0	0.2727(6)	0.54(8)	1 <sup>d</sup>
$Ln_1$ : Pr,Ce	$2b$	$\frac{1}{2}$	0	0.3829(7)	0.08(7) <sup>b</sup>	0.5/0.5 <sup>d</sup>
$Ln_2$ : Pr,Ce	$2a$	0	0	0.5403(6)	0.08(7) <sup>b</sup>	0.5/0.5 <sup>d</sup>
Cu <sub>2</sub>	$2b$	$\frac{1}{2}$	0	0.6505(6)	0.48(10)	1 <sup>d</sup>
Sr, Ba <sub>2</sub>	$2a$	0	0	0.7568(5)	0.50(15)	0.47/0.53 <sup>c</sup>
Cu <sub>3</sub>	$2b$	$\frac{1}{2}$	0	0.8997(5)	1.72(17)	1 <sup>d</sup>
O <sub>1</sub> <sup>a</sup>	$8f$	0.5699(29)	0.0667(30)	0.0060(6)	1.06(22)	0.25 <sup>d</sup>
O <sub>2</sub>	$2a$	0	0	0.1294(9)	2.20(21) <sup>e</sup>	1 <sup>d</sup>
O <sub>3</sub>	$4c$	$\frac{1}{4}$	$\frac{1}{4}$	0.2769(5)	1.20(11)	1 <sup>d</sup>
O <sub>4</sub>	$4c$	$\frac{1}{4}$	$\frac{1}{4}$	0.4567(6)	1.39(5)	1 <sup>d</sup>
O <sub>5</sub>	$4c$	$\frac{1}{4}$	$\frac{1}{4}$	0.6290(4)	0.67(9)	1 <sup>d</sup>
O <sub>6</sub>	$2b$	$\frac{1}{2}$	0	0.7852(8)	1.97(19)	1 <sup>d</sup>
O <sub>7</sub>	$4c$	$\frac{1}{4}$	$\frac{1}{4}$	0.8997 <sup>f</sup>	1.00 <sup>f</sup>	0 <sup>d</sup>
O <sub>8</sub>	$2a$	0	0	0.8997 <sup>f</sup>	1.00 <sup>f</sup>	0 <sup>d</sup>

Note.  $R_p = 5.55\%$ ,  $R_{wp} = 6.66\%$ ,  $R_{exp} = 2.75\%$ ,  $R_i = 6.16\%$ ,  $R_f = 5.03\%$ .

<sup>a</sup> Deviated from the  $(2b)$  position  $[\frac{1}{2}, \frac{1}{2}, 0.0060]$ .

<sup>b</sup> Refined simultaneously.

<sup>c</sup> Fixed from the X-ray powder diffraction refinement.

<sup>d</sup> Refined in first step and fixed after.

<sup>e</sup> Refined also in the  $(8f)$  position:  $[0.0349(29), 0.0193(53), 0.1284(8)]$ ,  $B = 0.84(28)$  Å<sup>2</sup>, and  $\tau = 0.25$ , but does not give significant improvement for the reliability factors.

<sup>f</sup> Empty positions at Cu<sub>3</sub> level.

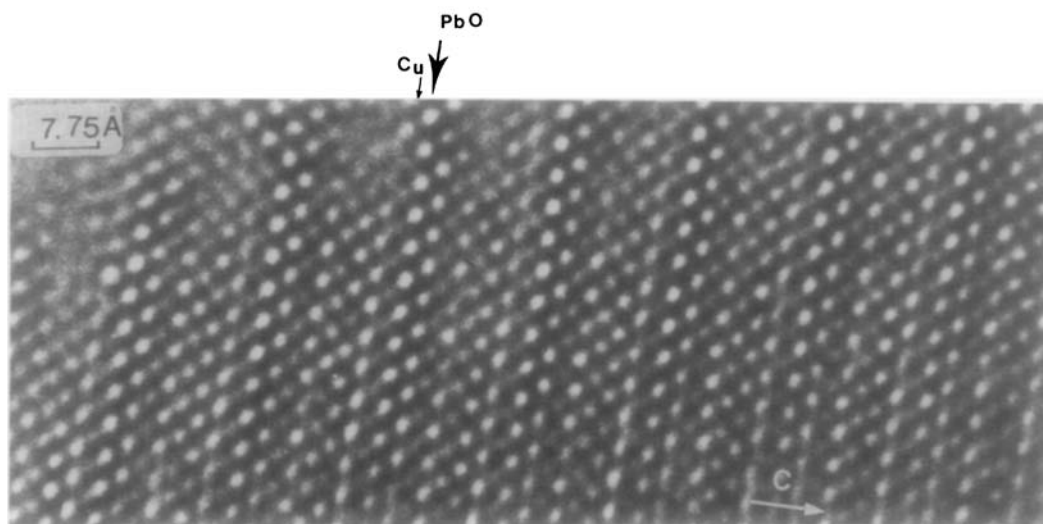


FIG. 6.  $[100]_r$  high resolution electron microscopy image of  $\text{PbBa}_{0.8}\text{Sr}_{1.2}\text{PrCeCu}_3\text{O}_9$ . The contrast is highly regular overall large areas; no domain or systematical variation of the contrast at the level of the copper and lead layers are observed (arrowed).

TABLE III  
INTERATOMIc DISTANCES (IN Å) IN  
PbBa<sub>0.77</sub>Sr<sub>1.23</sub>PrCeCu<sub>3</sub>O<sub>9</sub>

Pb-O <sub>1</sub>	2.39(2) [×1]	Ln <sub>2</sub> -O <sub>4</sub>	2.37(1) [×4]
	2.40(2) [×1]	-O <sub>5</sub>	2.42(1) [×4]
	3.12(2) [×1]		
	3.15(2) [×1]	Cu <sub>2</sub> -O <sub>5</sub>	1.97(1) [×4]
-O <sub>2</sub>	2.12(1) [×1]	-O <sub>6</sub>	2.21(2) [×1]
Sr, Ba <sub>1</sub> -O <sub>1</sub>	2.55(1) [×1]	Sr, Ba <sub>2</sub> -O <sub>5</sub>	2.85(1) [×4]
-O <sub>2</sub>	2.78(1) [×2]	-O <sub>6</sub>	2.78(1) [×2]
	2.77(1) [×2]		2.77(1) [×2]
-O <sub>3</sub>	2.75(1) [×4]		
		Cu <sub>3</sub> -O <sub>6</sub>	1.88(2) [×1]
Cu <sub>1</sub> -O <sub>2</sub>	2.35(2) [×1]	-O <sub>1</sub>	1.82(1) [×1]
-O <sub>3</sub>	1.94(1) [×4]		
		angle between the Cu <sup>1</sup> -O: O <sub>1</sub> -Cu <sub>3</sub> -O <sub>6</sub> : 164°	
Ln <sub>1</sub> -O <sub>3</sub>	2.60(1) [×4]		
-O <sub>4</sub>	2.28(1) [×4]		

2.35 Å) than generally found for high  $T_c$  superconductors (2.5–2.6 Å).

(ii) The lead environment is highly asymmetric. One indeed observes five neighbors, involving three short distances (2.12–2.39–2.40 Å) and two much longer ones (3.12–3.15 Å). These Pb–O distances confirm, if needed, the divalent state of lead in this phase. These five oxygens surrounding Pb(II) form a strongly distorted “O<sub>5</sub>” pyramid (Fig. 8), which can only be considered

as an average environment of Pb(II) owing to the splitting of the O<sub>1</sub> sites. It is worth pointing out that lead does not sit in the basal plane of the pyramid but is displaced out of the “O<sub>1</sub>” plane along  $c$  of 0.10 Å, outside of the pyramid, i.e., in the opposite direction to its apical oxygen O<sub>2</sub>. The coordination of lead can better be described as a distorted tetrahedron PbO<sub>3</sub>L, whose apices correspond to the three nearest oxygens (O<sub>1</sub> and O<sub>2</sub>) forming a triangle and the 6s<sup>2</sup> lone pair L of Pb(II) pointing along the perpendicular to the triangle. This particular coordination of Pb(II), influenced by the stereoactivity of its 6s<sup>2</sup> lone pair, has previously been observed in the oxides Pb<sub>2</sub>Sr<sub>2</sub>YCu<sub>3</sub>O<sub>8</sub> (9, 10) and Pb<sub>2</sub>Ba<sub>2</sub>YCu<sub>3</sub>O<sub>8</sub> (11), whose structure is also characterized by the existence of distorted [PbO]<sub>∞</sub> rock-salt-type layers, adjacent to layers of Cu<sup>1</sup>O<sub>2</sub> sticks.

(iii) The two-fold coordination of univalent copper Cu<sub>3</sub> is characterized by Cu–O distances close to those observed for Cu(I) in Pb<sub>2</sub>Sr<sub>2</sub>YCu<sub>3</sub>O<sub>8</sub>-type structures (9–11). The important feature deals with the nonlinear character of the O–Cu–O bond which exhibits an angle of 164°. Such an angled O–Cu–O bond is exceptional, since it was only reported recently for the parent structure Pb<sub>2</sub>Ba<sub>2</sub>YCu<sub>3</sub>O<sub>8</sub> (11), whereas for the

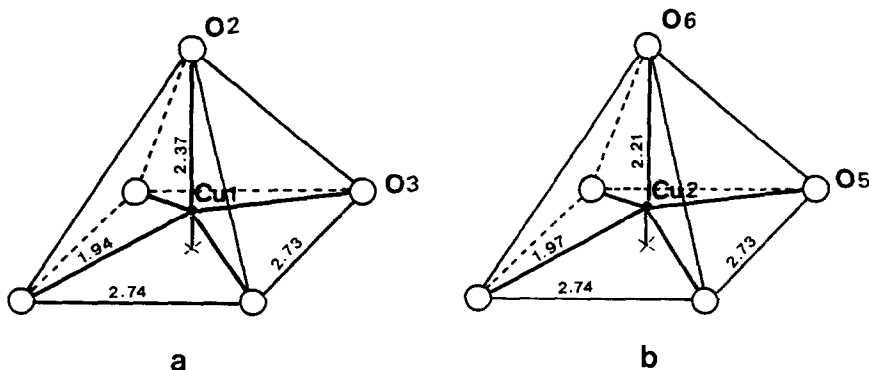


FIG. 7. Perspective drawing of the (a) Cu<sub>1</sub> and (b) Cu<sub>2</sub> pyramids. Distances are in angstroms.

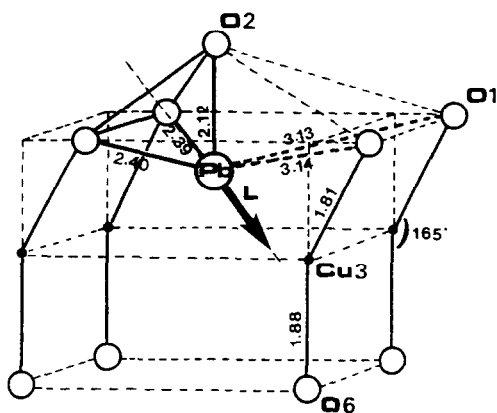


FIG. 8. Environment of Pb; the lone pair, L, is symbolized by a large black arrow. The distances are in angstroms.

isostructural oxide  $\text{Pb}_2\text{Sr}_2\text{YCu}_3\text{O}_8$  (9, 10) a linear bond was suggested. In fact, in the latter compound, the difficulty to detect a nonlinearity was due to the existence of a mirror plane and to the splitting of oxygen sites, on both sites of this mirror (9); the electron diffraction study of  $\text{Pb}_2\text{Ba}_2\text{YCu}_3\text{O}_8$  (11) allowed a different space group to be obtained without any mirror plane, leading after refinement to an angle of  $160^\circ$  for the O–Cu–O bond. In the present oxide, the asymmetry of the structure on both sides of  $\text{Cu}_3$  layer, leads to a primitive lattice which does not suffer any ambiguity about the geometry of this bond. These results show significantly the particular chemical bonding of Cu(I) in this oxide. Such a behavior may be the consequence of the

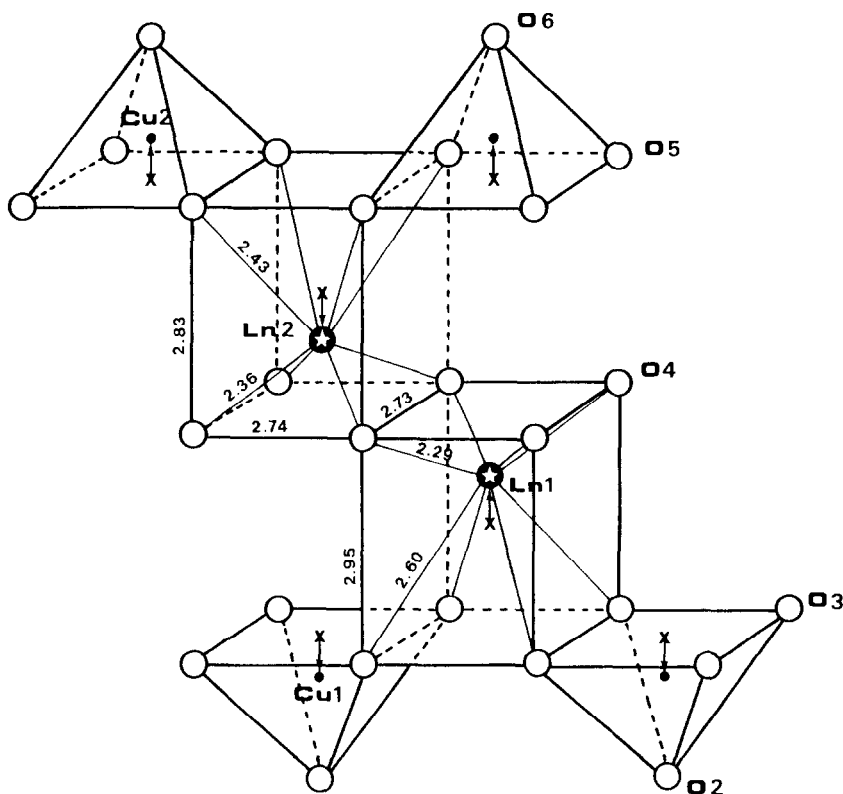


FIG. 9. Double fluorite cages located between the copper pyramidal layers. The distances are in angstroms.

stereoactivity of the  $6s^2$  lone pair of Pb(II), which tends to shift the oxygens in the PbO layers. Moreover, the Pb(II) lone pair which points out toward the  $\text{Cu}_3$  layer may also influence the geometry of the O–Cu–O bond.

(iv) The fluorite cages are slightly elongated along  $c$ , with O–O distances of 2.73–2.74 Å in the basal planes and O–O distances of 2.83–2.95 Å along  $c$ . A remarkable feature of this structure deals with the fact that the rare earth ions (Pr, Ce) are off-centered in their “ $\text{O}_8$ ” cage, leading to a  $4 + 4$  coordination, contrary to yttrium in  $\text{Pb}_2\text{Sr}_2\text{YCu}_3\text{O}_8$ -type structures for which eight equal Y–O bonds are always observed (9–11). This behavior seems to be a characteristic of the double fluorite-type layers. As shown from Fig. 9, praseodymium and cerium ions tend to move away from the copper planes ( $\text{O}_3$  and  $\text{O}_5$  planes) toward the intermediate  $\text{O}_4$  plane, which does not contain cations.

Another interesting issue concerns the  $L_n$ –O distances corresponding to  $L_{n_1}$  in 2( $b$ ) sites which are longer than those corresponding to  $L_{n_2}$  in 2( $a$ ) sites. This suggests that 2( $b$ ) sites would be preferentially occupied by Pr(III) and 2( $a$ ) sites by Ce(IV) if one takes into account the relative sizes of these elements. However, bond valence calculations do not support this viewpoint, as shown above.

## References

1. C. MARTIN, D. BOURGAULT, M. HERVIEU, C. MICHEL, J. PROVOST, AND B. RAVEAU, *Mod. Phys. Lett. B* **3**, 993 (1989).
2. J. AKIMITSU, S. SUZUKI, M. WATANABE, AND H. SAWA, *Jpn. J. Appl. Phys.* **27**, L 1859 (1988).
3. H. SAWA, S. SUZUKI, M. WATANABE, J. AKIMITSU, H. MATSUBARA, H. WATABE, S. UCHIDA, K. KOKUSHO, H. ASANO, F. IZUMI, AND E. TAKAYAM-MUROMACHI, *Nature* **337**, 347 (1989).
4. Y. TOKURA, T. ARIMA, H. TAKAGI, S. UCHIDA, T. ISHIGAKI, H. ASANO, R. BEYERS, A. I. NAZZAL, P. LACORRE, AND J. B. TORRANCE, *Nature* **342**, 890 (1989).
5. T. ROUILLON, D. GROULT, M. HERVIEU, C. MICHEL, AND B. RAVEAU, *Phys. C* **167**, 107 (1990).
6. H. SAWA, K. OBARA, J. AKIMITSU, Y. MATSUI, AND S. HORIUCHI, *J. Phys. Soc. Jpn.* **58**, 2252 (1989).
7. T. WADA, A. ICHINOSE, Y. YAEGASHI, H. YAMAUCHI, AND S. TANAKA, *Phys. Rev. B* **41**, 1984 (1990).
8. A. TOKIWA, T. OKU, M. NAGOSHI, D. SHINDO, M. KIKUCHI, T. OIKAMA, K. HIRAGA, AND Y. SYONO, *Phys. C* **172**, 155 (1990).
9. R. J. CAVA, M. MAREZIO, J. J. KRAJEWSKI, W. F. PECK, A. SANTORO, AND F. BEECH, *Phys. C* **157**, 272 (1989).
10. U. AMADOR, F. GARCIA-ALVADARO, F. MORAN, M. A. ALARIO-FRANCO, AND J. RODRIGUEZ-CARJAVAL, *Phys. C* **165**, 499 (1990).
11. W. T. FU, H. W. ZANDBERGEN, N. G. HAIJE, AND J. L. DE JONGH, *Phys. C* **159**, 210 (1989).
12. W. H. ZACHARIASEN, *J. Less-Common Met.* **62**, 1 (1978).
13. I. D. BROWN AND D. ALTERMATT, *Acta Crystallogr., Sect. B: Struct. Sci* **41**, 244 (1985).
14. D. B. WILES AND R. A. YOUNG, *J. Appl. Crystallogr.* **14**, 149 (1981).